

pHTomato, a red, genetically encoded indicator that enables multiplex interrogation of synaptic activity

Yulong Li¹ & Richard W Tsien^{1–4}

The usefulness of genetically encoded probes for optical monitoring of neuronal activity and brain circuits would be greatly advanced by the generation of multiple indicators with non-overlapping color spectra. Most existing indicators are derived from or spectrally convergent on GFP. We generated a bright, red, pH-sensitive fluorescent protein, pHTomato, that can be used in parallel with green probes to monitor neuronal activity. SypHTomato, made by fusing pHTomato to the vesicular membrane protein synaptophysin, reported activity-dependent exocytosis as efficiently as green reporters. When expressed with the GFP-based indicator GCaMP3 in the same neuron, sypHTomato enabled concomitant imaging of transmitter release and presynaptic Ca²⁺ transients at single nerve terminals. Expressing sypHTomato and GCaMP3 in separate cells enabled the simultaneous determination of presynaptic vesicular turnover and postsynaptic sub- and supra-threshold responses from a connected pair of neurons. With these new tools, we observed a close size matching between pre- and postsynaptic compartments, as well as interesting target cell-dependent regulation of presynaptic vesicle pools. Lastly, by coupling expression of pHTomato- and GFP-based probes with distinct variants of channelrhodopsin, we provided proof-of-principle for an all-optical approach to multiplex control and tracking of distinct circuit pathways.

Genetically encoded indicators have greatly advanced our ability to understand the complex physiology of neurons by allowing non-invasive monitoring of a variety of activity-regulated signals, including membrane potential^{1,2}, Ca²⁺ (refs. 3,4), Cl⁻ (ref. 5) and transmitter release^{6,7}. Regrettably, most existing optical probes, which are based on GFP or on fluorescence resonance energy transfer (FRET) between a pair of fluorescent proteins, have a large degree of spectral overlap that precludes them from being used in a multiplex fashion. The development of indicators that can be used in combination with GFP-based indicators would allow, for example, simultaneous imaging of multiple classes of neurons to understand information processing, or of pre- and postsynaptic activity to isolate the locus of different types of synaptic plasticity. In addition, recent breakthroughs with optogenetic agents such as channelrhodopsin-2 and halorhodopsin provide powerful ways to start or stop neuronal firing^{8–10}. Combining these

optical tools for controlling circuit function with new optical indicators of activity would greatly enhance our ability to explore the natural behavior of neurons and synapses. Pioneering work has harnessed a pH-sensitive variant of GFP, pHluorin, fused to a vesicle protein, VAMP2, to probe the turnover of synaptic vesicles⁶. When a vesicle undergoes exocytosis, the pH of the vesicle lumen changes from 5.5 to 7.4, causing pHluorin-based probes exposed to the vesicle lumen to increase their fluorescence, thereby reporting presynaptic vesicle turnover. Color variants of pHluorin would complement the many GFP-based probes and allow dual-channel acquisition of images. A prime candidate, the mOrange mutant M163K, has a suitable pK_a of 7.5 (ref. 11) but displays undesirable photoswitching behavior¹² and correspondingly poor performance in imaging transmitter release. Other color variants of fluorescent proteins, including mKate, are spectrally distinct from GFP but sometimes display photoswitching behavior¹², and they have a pK_a of 6.0 (ref. 13), not optimal for detection of vesicle exocytosis¹⁴. Accordingly, we set out to develop a pH-sensitive indicator protein, spectrally distinct from GFP, with a pK_a specifically tuned to report vesicle exocytosis.

RESULTS

Starting with the monomeric red fluorescent proteins mRFP and mStrawberry^{15,16}, we performed DNA shuffling and semi-random mutagenesis (see Online Methods). Through three rounds of evolution, we identified a bright, pH-sensitive mutant (**Fig. 1**), termed pHTomato because its excitation (550 nm) and emission (580 nm) peaks are similar to those of Tomato variants from the mFruit series¹⁶. pHTomato contains six amino acid differences from mStrawberry (F41T, F83L, S182K, I194K, V195T and G196D). Notably, pHTomato contains a critical threonine at position 66 and is thus reminiscent of mRFP-Q66T¹⁷.

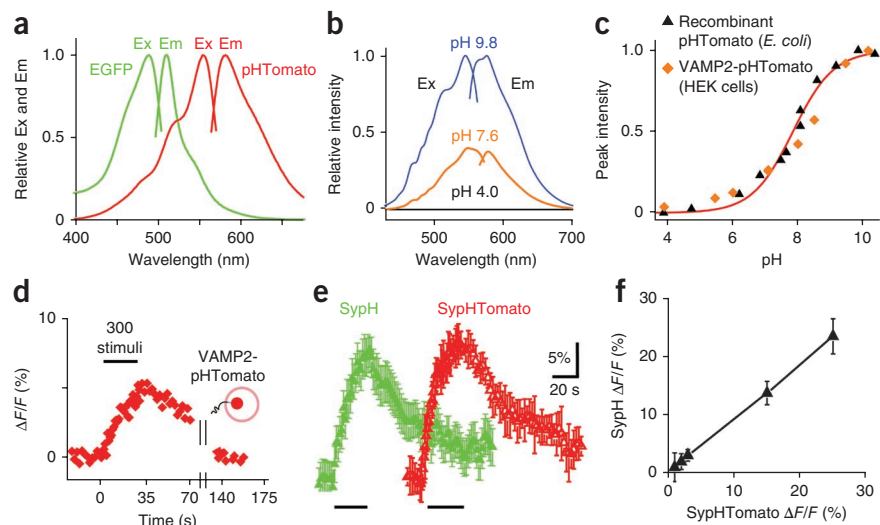
Cuvette measurements of recombinant pHTomato (**Fig. 1a** and **Supplementary Fig. 1b**) demonstrated that it was highly pH sensitive, with a pK_a close to 7.8 (**Fig. 1b,c**). Notably, although the emission intensity of pHTomato showed strong pH dependence, its excitation and emission waveforms were pH independent (**Fig. 1b**). Such spectral stability is critical for straightforward multiplexing of pHTomato with genetically encoded indicators of other colors.

We fused pHTomato to the luminal domain of VAMP2 and characterized its properties in mammalian cells. When expressed in human

¹Department of Molecular and Cellular Physiology, Stanford University School of Medicine, Stanford, California, USA. ²NYU Neuroscience Institute, New York University, New York, New York, USA. ³Department of Physiology and Neuroscience, New York University, New York, New York, USA. ⁴Center for Neural Science, New York University, New York, New York, USA. Correspondence should be addressed to Y.L. (yulong@gmail.com) or R.W.T. (richard.tsien@nyumc.org).

Received 7 March; accepted 30 April; published online 27 May 2012; doi:10.1038/nn.3126

Figure 1 pHTomato spectra and properties. (a) Excitation (Ex) and emission (Em) spectra for EGFP³⁷ and pHTomato. Spectral peaks of pHTomato (excitation, 550 nm; emission 580 nm) are well separated from those of EGFP. (b) pH dependence of pHTomato fluorescence, showing no change in wavelength of excitation and emission peaks. (c) Normalized fluorescence intensities of recombinant pHTomato (produced in *Escherichia coli*; black triangles) and VAMP2-pHTomato (expressed in HEK cells; orange diamonds) were both highly pH dependent, with identical values of pK_a (7.8 ± 0.1). (d) VAMP2-pHTomato–reported, activity-dependent exo- and endocytosis in cultured hippocampal neurons, reflected by stimulus-driven rise and fall in relative fluorescence signal over baseline ($\Delta F/F$). Inset shows a labeled synaptic vesicle. (e) Quantification of fluorescence signals from sypH and sypHTomato, expressed in the same neuron. The two probes performed equally well in reporting presynaptic activity as $\Delta F/F$. Data obtained by averaging responses of 110 boutons (300 stimuli at 10 Hz). Traces displaced horizontally for clarity. (f) Comparison of sypH and sypHTomato signals under different stimulation conditions, ranging from 5 to 1,200 stimuli ($n = 6$ neurons, ~ 700 boutons), shows their proportional and nearly equal responses. All error bars are s.e.m.



embryonic kidney (HEK) cells, the VAMP2-pHTomato fusion showed a pH dependence that was identical to that of recombinant pHTomato alone (Fig. 1c), indicating that fusion to VAMP2 did not perturb the pH sensitivity of pHTomato. In addition, when expressed in primary cultures of rat hippocampal neurons, VAMP2-pHTomato showed reversible fluorescence increases in response to field stimulation (Fig. 1d), demonstrating the capability of VAMP2-pHTomato to report synaptic vesicle exo- and endocytosis.

Knowing that synaptophysin displays less background expression on the plasma membrane than VAMP2 (refs. 18,19), we used synaptophysin as the basis for an improved reporter of vesicular turnover, sypHTomato. We inserted the pHTomato sequence into the middle of the open reading frame, directing the pHTomato moiety toward the vesicular lumen. To confirm that overexpression of sypHTomato does not alter vesicle turnover, we used activity-dependent FM styryl dye uptake and destaining as an independent assay of endo- and exocytosis. Dye uptake in sypHTomato-positive nerve terminals and untransfected controls were statistically indistinguishable ($P > 0.1$; Supplementary Fig. 2). Moreover, we observed a near-perfect overlap of the destaining trajectories for sypHTomato-transfected cells relative to control cells upon further stimulation to release the FM dye (Supplementary Fig. 2). Thus, sypHTomato overexpression does not produce deleterious effects on vesicular dynamics.

We subsequently expressed sypHTomato with synaptophysin-pHluorin (sypH) for a direct comparison of their performance in the same hippocampal neurons (Fig. 1e). Despite the slightly higher pK_a of pHTomato (7.8) relative to that of pHluorin (~ 7.3 ; refs. 6,14), sypHTomato and sypH performed nearly equally well in reporting synaptic vesicle fusion, consistent with theoretical considerations¹⁴. The peak height of the fluorescence signal from sypHTomato correlated well with that of sypH over a wide range of activity (Fig. 1f). We performed NH_4Cl dequenching experiments¹⁴ and estimated the surface fraction of sypHTomato at rest to be $8.1 \pm 1.2\%$ ($n = 207$ synapses, four experiments), similar to that of sypH reported previously ($7.5 \pm 1.1\%$ (ref. 18), $9.1 \pm 0.6\%$ (ref. 19)). Finally, the signal-to-noise ratio was similar for the two probes, and each was able to detect exocytosis elicited by as few as five stimuli. Therefore, sypHTomato is a robust, genetically encoded indicator with capabilities matching those of existing probes.

Imaging vesicular turnover and Ca^{2+} in same synapses

The two-color capability provides an immediate advantage in clarifying the intricate relationship between vesicle fusion and presynaptic calcium signaling. Both processes can be imaged concurrently in single nerve terminals by using sypHTomato along with green calcium indicators such as GCaMP3 (refs. 20,21). In cultured hippocampal neurons transfected with sypHTomato and GCaMP3, sypHTomato was found to be highly enriched in presynaptic boutons, whereas GCaMP3 was distributed more diffusely (Supplementary Fig. 1c). In response to depolarizing field stimulation (10 Hz, 10 s), we observed transient increases in both GCaMP3 and sypHTomato fluorescence (Fig. 2a). We quantified the responses from a single neuron (Fig. 2a) with respect to both time (Fig. 2b) and location (Supplementary Fig. 1d). Further analysis revealed that the sypHTomato and GCaMP3 responses showed distinct temporal patterns in various neuronal compartments: presynaptic puncta (Fig. 2a), interbouton regions (Fig. 2a) and somata (Supplementary Fig. 1d). Presynaptic boutons were defined by subsequent NH_4Cl challenge, which imposed an influx of NH_3 to neutralize intracellular compartments²² (see Online Methods). Whereas we observed GCaMP3 responses in both presynaptic terminals and interbouton regions (Fig. 2a), the sypHTomato response was confined to the presynaptic puncta (Fig. 2a). However, the GCaMP3 response at the time of stimulation was considerably enhanced in the vicinity of sypHTomato responses ($P < 0.01$, bouton versus interbouton; Fig. 2b), as also seen in plots of fluorescent intensity along the length of an axon (Supplementary Fig. 1d). The close spatial overlap of the two signals is consistent with the well documented enrichment of voltage-gated calcium channels in synaptic boutons. Lateral spread of Ca^{2+} from the synaptic regions to the interbouton regions was presumably attenuated by sequestration and extrusion.

This dual-color optical imaging approach allows calcium levels and presynaptic release to be compared directly at the same synapses. We progressively varied the number of stimuli (5 to 60 stimuli, 20 Hz) and simultaneously monitored presynaptic GCaMP3 ($GCaMP3_{pre}$) and sypHTomato signals (Fig. 2c). When these signals were scaled to allow comparison of their kinetics, the decay phase of the sypHTomato signal significantly outlasted the transient $GCaMP3_{pre}$, declining ~ 10 times more slowly (Fig. 2d). The decay kinetics of sypHTomato

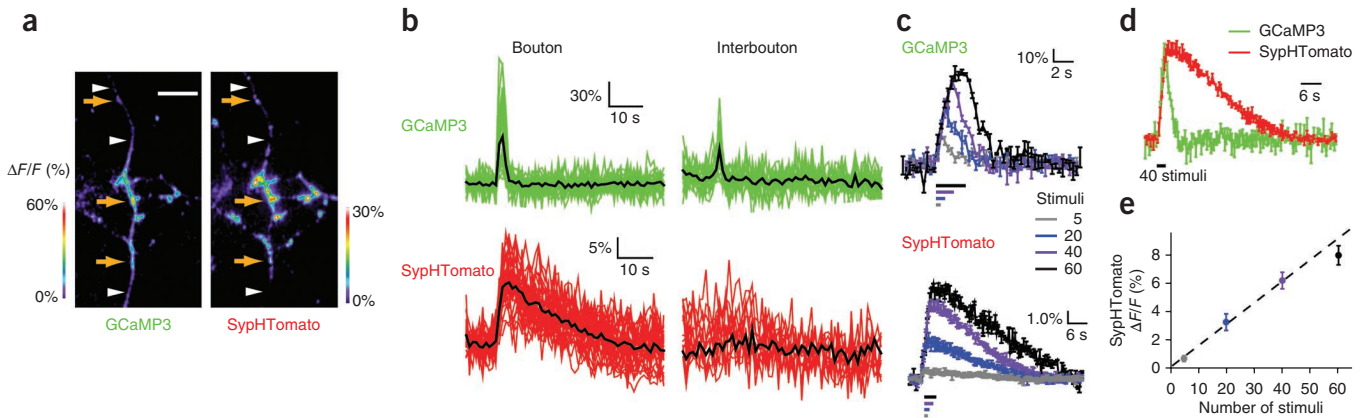


Figure 2 Dual-color simultaneous imaging of vesicle fusion and cytosolic Ca^{2+} . (a) Pseudocolor snapshots of $\Delta F/F$ fluorescence signals evoked by 100 stimuli (10 Hz) for GCaMP3 and syphTomato, respectively. Arrows, putative presynaptic boutons; arrowheads, interbouton regions. Scale bar, 10 μm . (b) Collection of GCaMP3 and syphTomato responses over time from 20 putative presynaptic boutons (randomly selected out of 152 total) and corresponding adjacent interbouton regions $\sim 2\text{--}5 \mu\text{m}$ away. Averages of individual traces shown in black. Responses evoked with 40 stimuli at 20 Hz. Data are from cell in a. (c) Average GCaMP3 and syphTomato $\Delta F/F$ signals from a set of synapses in response to trains of 5, 20, 40 and 60 stimuli (20 Hz). Each trace represents pooled data from ~ 600 boutons on five different coverslips. (d) Comparison of kinetics of GCaMP3 and syphTomato signals in response to 40 stimuli at 20 Hz. The decay of normalized syphTomato signal ($\tau = 15.5 \pm 0.5 \text{ s}$) significantly outlasted that of the presynaptic GCaMP3 response ($\tau = 1.5 \pm 0.14 \text{ s}$). (e) Quantification of peak amplitudes of syphTomato responses. All data conform to regression line passing through the origin, showing linear increase with the number of stimuli, aside from the falloff at 60 stimuli. Thus, response amplitude per action potential stays the same up to 40 stimuli ($P > 0.2$). All error bars are s.e.m.

signals arising from 5 stimuli were very similar to those arising from 40 (Supplementary Fig. 1e). Evidently, the ensemble rate of endocytosis was not appreciably altered by moderate increases in neuronal activity under our conditions. To determine how the amount of exocytosis per action potential varies with activity, we plotted the peak amplitude of syphTomato signal as a function of the number of stimuli (Fig. 2e). The amplitude increased linearly up to 40 stimuli, corresponding to a nearly constant amount of vesicular turnover per action potential, $0.16 \pm 0.06\%$ per action potential at 20 Hz. From the vantage point of neural signaling, this provides a compact description of how a number of action potentials can be encoded as the extent of exocytosis.

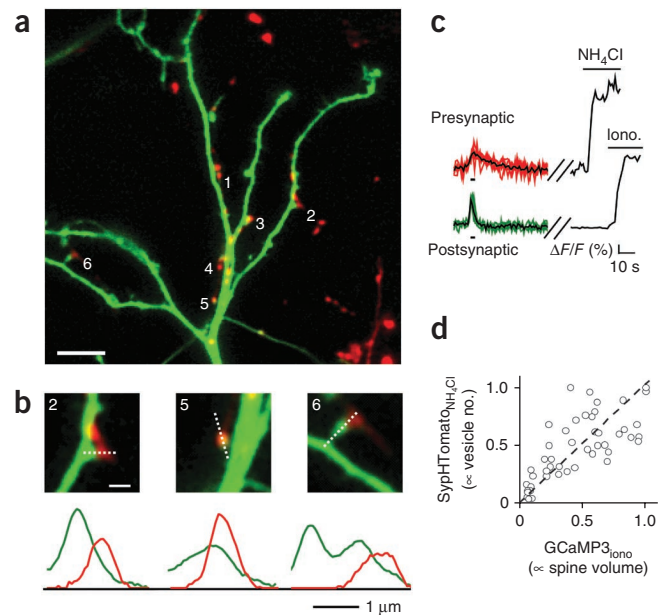
We went on to test whether larger synapses are particularly enriched in a specific channel type, using specific toxins to dissect the contributions of various voltage-gated Ca^{2+} channel types. The average contributions of the channels were notably consistent among synapses of different size within the same axonal tree studies (see Supplementary Figs. 3 and 4). We found no evidence for a bimodal distribution of channel types in which some synapses completely lacked P/Q- or

N-type channels. It is conceivable that previous studies in similar hippocampal culture systems^{23,24} may have included contributions from inhibitory nerve terminals, now known to rely on either P/Q- or N-type channels to the exclusion of the other.

Imaging chemical transmission from connected neurons

SyphTomato enabled us to visualize synaptic transmission from a presynaptic terminal onto a postsynaptic cell in a wholly optical system. Traditional approaches have often been limited to either pre- or postsynaptic optical measurements, or they have used electrophysiology, which lacks some advantages of genetically encoded indicators. We expressed syphTomato and GCaMP3 in separate hippocampal neurons (see Online Methods) and looked for synaptic contacts

Figure 3 Dual-color imaging of synaptic connection by syphTomato and GCaMP3. (a) Image of a pair of connected neurons (20 d *in vitro*) where pre- and postsynaptic neurons expressed syphTomato (red) and GCaMP3 (green). Regions 1–6 highlight putative synapses. Scale bar, 10 μm . (b) Enlarged views of regions 2, 5 and 6 illustrating morphology and close proximity between presynaptic boutons (red) and postsynaptic spines (green). Intensity distributions along scan lines (dotted) plotted below. Note spatial overlap between red and green profiles as expected for apposed structures and image dimensions near the diffraction limit. Scale bars, 1 μm . (c) Representative responses from a single synapse. Presynaptic syphTomato (top) responded to 40 stimuli (bar, bottom left) and subsequent NH_4Cl challenge; postsynaptic GCaMP3 responded to the same 40 stimuli and to Ca^{2+} permeabilization with ionomycin (Iono., bottom). Black traces, average responses to five trials of 40 stimuli. Scale bar for $\Delta F/F$: 10% for syphTomato, 40% for GCaMP3. (d) Amplitude of peak responses of syphTomato upon NH_4Cl challenge plotted against corresponding peak amplitudes of GCaMP3 responses in the presence of ionomycin. Data from seven pairs of neurons were normalized by largest response for each pair, then pooled.



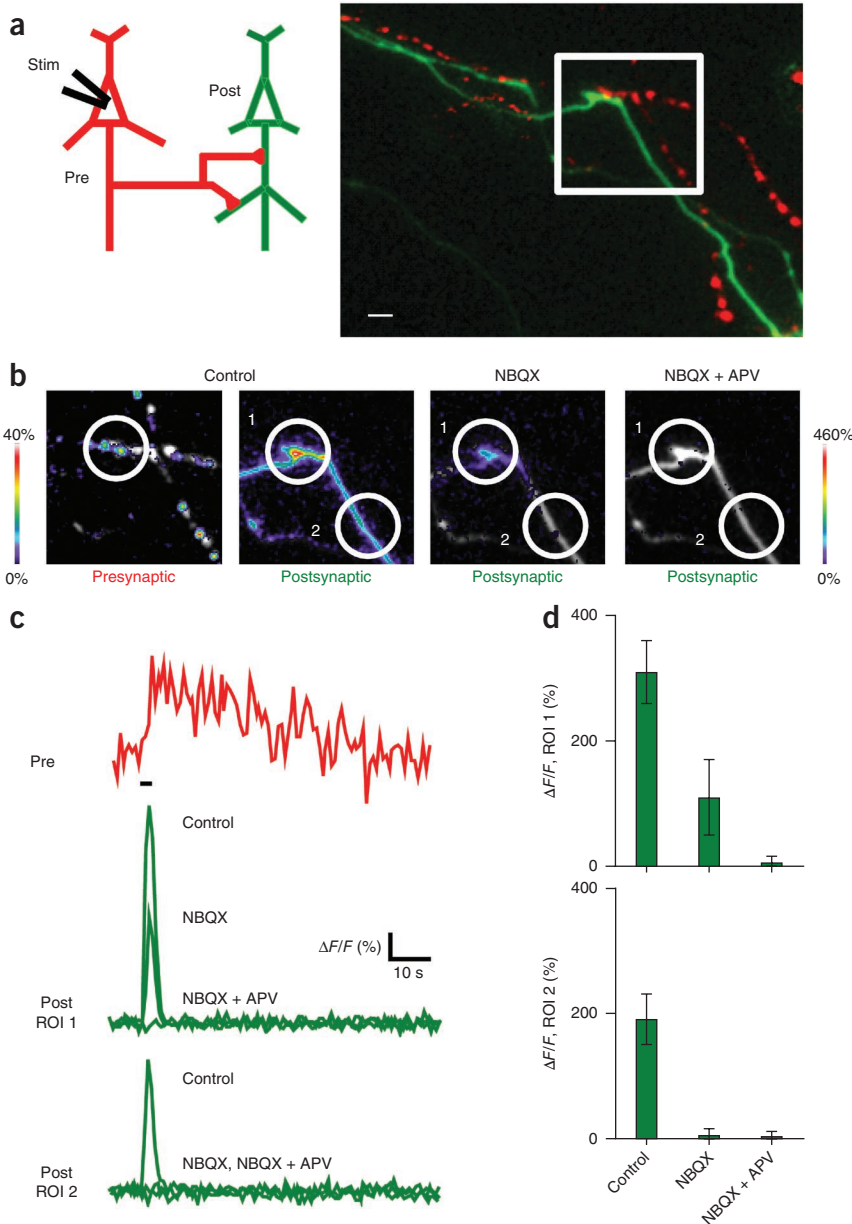


Figure 4 Dynamic imaging of synaptic transmission in suprathreshold or subthreshold condition by presynaptic sypHTomato and postsynaptic GCaMP3. **(a)** A diagram showing a connected pair of neurons (left), and an experimental image (right) showing the spatial arrangements between presynaptic sypHTomato signal (red) and postsynaptic neuron (green) under study. Stim, stimulation; Pre, presynaptic cell; Post, postsynaptic cell. Scale bar, 1 μ m. **(b)** Pseudocolor snapshots from outlined region in **a**, showing peak responses by 40 stimuli at 20 Hz in the sypHTomato (presynaptic) and GCaMP3 (postsynaptic) channels. Note the close proximity between presynaptic sypHTomato and postsynaptic GCaMP3 signal in circled region of interest (ROI) 1. ROI 2 is a neighboring region of postsynaptic dendrite lacking presynaptic contact. **(c)** Quantification of time lapse results from **b** in control, NBQX and NBQX + APV conditions (see Online Methods). Scale bar for $\Delta F/F$: 15% for sypHTomato, 60% for GCaMP3. **(d)** Quantification of group data from pairs of connected neurons, from experiments similar to those in **b, c** ($n = 5$ pairs for NBQX condition, $n = 11$ for both control and NBQX + APV conditions). ROI 2 was typically 4–7 μ m from ROI 1. Error bars, s.e.m.

fluorescence signal increase provided a rough indication of the total number of presynaptic vesicles. Similarly, we monitored the postsynaptic response to the same burst of exocytosis and then monitored the increase of GCaMP3 signal in the presence of ionomycin (**Fig. 3c**, bottom), a selective calcium ionophore that raises Ca^{2+} uniformly throughout the cell. The amplitude of the ionomycin response served as a proxy for postsynaptic spine volume.

We next sought to determine whether correlations exist between pre- and post-synaptic compartments. Plotting the presynaptic sypHTomato signal against the corresponding postsynaptic GCaMP3 signal at individual synapses revealed a high degree of 'size

matching'^{26,27} between presynaptic compartment and postsynaptic target (**Fig. 3d**, correlation coefficient $R = 0.8$).

Do presynaptic neurons act in a cell-autonomous manner to distribute their synaptic vesicles between different target cells, or is this allocation also dependent on the target? Taking advantage of the dual-color photometry approach, we divided presynaptic terminals arising from a sypHTomato-labeled neuron into those that targeted a particular postsynaptic neuron and those that did not. We quantified of sizes of total vesicle pools (probed by NH_4Cl) and readily releasable pools (probed by 40 stimuli, 20 Hz). Presynaptic boutons sharing the same postsynaptic neuron were more consistent in s.d. than other presynaptic terminals from the same axon. Notably, we found that presynaptic boutons sharing the same postsynaptic target neuron had similar vesicular abundance ($n = 43$ synapses, 7 neurons), with a relatively small scatter in their NH_4Cl -evoked vesicular signal (relative s.d. = 0.4 ± 0.1 , $P < 0.05$, t test), compared to nerve terminals targeting an assortment of postsynaptic neurons (relative s.d. = 1 ± 0.2 , $n = 141$ synapses). The vesicles in the readily releasable pool also

between sypHTomato-positive terminals and GCaMP3-positive dendrites (**Fig. 3a**). Putative contact sites (**Fig. 3b**) displayed characteristic morphology, with prominent presynaptic varicosities (red) lying in close proximity to GCaMP3-positive postsynaptic structures (green). In functional recordings that capitalized on the sensitivity of the optical probes, we found that most of the putative contacts were *bona fide* active synapses (postsynaptic Ca^{2+} rises detected in 51 out of 63 putative synapses in 11 neurons). Closer examination of individual synapses revealed that most of the presynaptic boutons innervated spine-like postsynaptic structures (**Fig. 3a,b**). The fraction of nerve terminals that targeted spines increased with synapse maturation (**Supplementary Fig. 5c**), as expected for hippocampal excitatory synapses.

We functionally characterized individual synaptic contacts with a combination of electrical stimulation and pharmacological intervention. Electrical stimulation of presynaptic somata sufficient to drive the turnover of the readily releasable pool of vesicles (40 stimuli at 20 Hz; ref. 25) was followed by a pulse of NH_4Cl , to transiently decacidify the entire synaptic vesicle compartment (**Fig. 3c**, top). The resulting sypHTomato

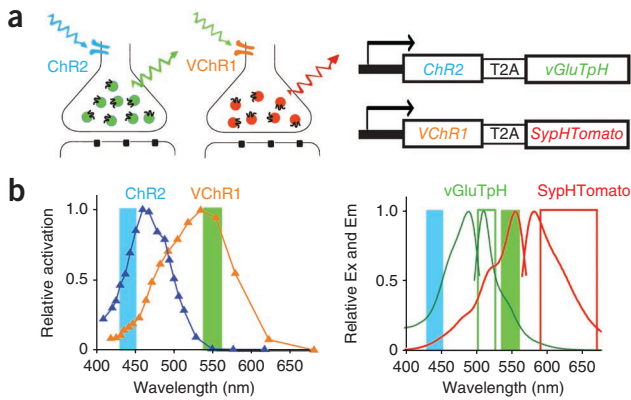


Figure 5 Proof of principle for an all-optical control and readout system.

(a) Schematic illustrating how vGluTpH and sypHTomato can work in a multiplex way in conjunction with variants of channelrhodopsin (left) expressed from genes joined in tandem by T2A linkers (right). Cell surface-targeted ChR2 can be co-expressed with vesicularly targeted vGluTpH; blue light serves to both activate ChR2 and excite vGluTpH (green) to probe synaptic activity. VChR1 (orange) and sypHTomato (red) can be combined in a similar but orthogonal fashion along with green light. (b) The activation spectra of ChR2 and VChR1 (left)⁹ show extensive overlap with the excitation spectra of vGluTpH or sypHTomato (right). Filled blue and green bars show the spectra of light (426–450 nm or 546–566 nm) used to activate ChR2 and VChR1, respectively. The same light was used to excite (Ex) vGluTpH and sypHTomato, respectively. Open green and red rectangles indicate the emission (Em) filters for vGluTpH and sypHTomato, respectively. (c) Expression of ChR2-T2A-vGluTpH leads to robust blue light-dependent exocytosis (center), similar to that produced by direct electrical stimulation (left). TTX abolishes the light-dependent response (right), demonstrating the requirement for excitability and subsequent opening of voltage-gated calcium channels. *f*, frequency (rate) of light pulses. (d) Similar and complementary experiments using VChR1-T2A-sypHTomato. (e) Blue light was unable to activate vChR1 to evoke sypHTomato responses (center), whereas both green light (right) and electric stimulation (left) induced robust responses. Notably, cross-talk is not an issue for the opposite combination because green light overlaps minimally with the ChR2 activation spectrum and with pHluorin's excitation spectrum (b). Results shown are data from a single neuron (average responses from 100 to 150 boutons). Experiments were repeated in 4–7 neurons for each condition.

showed a similar trend (relative s.d. = 0.6 ± 0.2 , $P < 0.05$). In comparison, the fraction of readily releasable pool per total vesicle pool (0.27 ± 0.15 and 0.25 ± 0.11), expressed as ratio of the peak responses to 40 stimuli (20 Hz) and to NH_4Cl , did not differ according to targets ($P > 0.1$, *t* test). Because all the labeled nerve terminals arose from the same presynaptic neuron, the more precise allocation of synaptic vesicles at synapses sharing the same target neuron relative to that at those with different target neurons implicates extrinsic signaling, possibly involving retrograde communication from the postsynaptic cell itself²⁸.

We next combined single-cell electrical stimulation with dual-color imaging to interrogate synaptic transmission directly (Fig. 4a). Stimulation with 40 pulses at 20 Hz near the soma of the presynaptic neuron resulted in a robust increase in fluorescence from sypHTomato terminals (Fig. 4b), consistent with the high reliability of action potential propagation. The postsynaptic glutamate receptors were in turn activated, leading to a nearly concurrent increase of the GCaMP3 signal in the postsynaptic dendrite. This was seen immediately adjacent to the presynaptic terminals and also throughout the dendrite (Fig. 4b,c). We interpreted this global dendritic calcium increase as an outcome of postsynaptic firing and opening of voltage-gated calcium channels throughout the neuron. To test this interpretation, we applied NBQX, a selective AMPA receptor antagonist, to reduce postsynaptic receptor activation and thus lower the drive for postsynaptic spikes. Indeed, NBQX confined the postsynaptic response, restricting it to the dendritic region just postsynaptic to the active terminal, with no calcium signal detected in a nearby postsynaptic region (Fig. 4b,c). We confirmed that this isolated calcium response was a result of NMDA receptor activation by verifying that APV, a selective NMDA receptor antagonist, completely abolished all postsynaptic responses (Fig. 4b,c). Thus, the all-optical approach was

capable of achieving single-synapse resolution robustly, as confirmed in several pairs of excitatory neurons (Fig. 4d).

Finally, with these color variants of activity probes in hand, we explored the possibility of using a multiplex optical strategy for both direct control and readout of neuronal activity. Such a combination of optical approaches is to our knowledge unprecedented, but it would be very powerful for noninvasive studies of synapse-specific regulation in neural circuits. This strategy is illustrated here by combining color variants of channelrhodopsin with probes of exocytosis with distinct spectral properties (Fig. 5a). Using a bicistronic T2A expression system⁹ to drive expression of genetically encoded agents (Fig. 5a, right), we introduced channelrhodopsin-2 (ChR2) and vGluTpH, a pHluorin-tagged vesicular glutamate transporter that specifically labels glutamate-containing vesicles²⁹, into the same cultured hippocampal neurons. The ChR2 and vGluTpH were both robustly expressed using the T2A linkage and correctly targeted to plasma membrane and synaptic vesicles, respectively. For proof of principle, we used a single beam of blue light (436–450 nm) to activate ChR2 and to interrogate vGluTpH (Fig. 5b); distinct wavelengths could be used for activation and interrogation under other circumstances (Supplementary Fig. 6b). The vGluTpH responded to exocytosis in excitatory neurons elicited by electrical field stimulation (40 Hz, 2 s; Fig. 5c, left). In the same cells, raising the frequency of blue light illumination (increasing from 0.3 Hz to 5 Hz for 20 s) caused a marked increase in vGluTpH signal, indicating enhanced vesicle turnover (Fig. 5c, center). The light-driven response was blocked by bath application of tetrodotoxin (TTX; Fig. 5c, right), demonstrating the requirement for action potentials (and subsequent opening of voltage-gated Ca^{2+} channels) to trigger vesicle fusion. In a similar experiment, the spectral alignment of VChR1 (ref. 9) and vesicularly targeted sypHTomato allowed

us to use a beam of green light (546–566 nm; **Fig. 5b**) to activate both VChR1 and sypHTomato (**Fig. 5d**). Once again, the synaptic monitor reported a light-driven, action potential–dependent increase in vesicular turnover. To assess the potential cross-talk between these two systems, we investigated the more difficult condition in which blue light might bleed through to activate VChR1, whose activation spectrum tails off incompletely in the blue (**Fig. 5b**). Delivering blue light to neurons transfected with VChR1-T2A-sypHTomato (**Fig. 5e**, left) did not evoke a detectable response even at double the light intensity (**Fig. 5e**, center). As a positive control, the same cells responded robustly to elevating the frequency of green light pulses (**Fig. 5e**, right). These data establish proof of principle for the application of T2A-linked expression of molecular tools in the control and readout of neural activity. The availability of spectrally distinct variants for both stimulation and recording enables an all-optical strategy for parallel use in distinct neuronal populations.

DISCUSSION

We have generated a bright, red, pH-sensitive, genetically encoded probe termed pHTomato and constructed indicators based on this probe that enable imaging of neurotransmitter release. The new molecules were designed to overcome several technical obstacles that hamper the ability of existing techniques to elucidate the mechanisms of presynaptic regulation. For example, conventional postsynaptic electrical recordings, though sensitive, can be complicated by passive cable filtering, postsynaptic receptor trafficking, saturation or desensitization. FM dye imaging is capable of directly assaying presynaptic function, but dye uptake generally occurs at all functional synapses, hampering experiments that require cell-type specificity. SynaptopHluorin directly monitors presynaptic activity and, being genetically encoded, provides neuronal specificity. However, it fluoresces in the green and thus has spectral properties that overlap those of many common probes. New indicators are clearly desirable to complement the strengths of existing probes for important signaling agents such as Ca^{2+} , cyclic AMP, inositol trisphosphates, nitric oxide, and activated kinases and phosphatases.

Our design strategy was to screen new molecules based on bright and monomeric red fluorescent proteins that were already available. We generated a variant library by combining DNA shuffling of mStrawberry and mRFP with random error-prone PCR throughout the molecule and screened bright mutants for optimal pH sensitivity. The newly generated indicator, pHTomato, is spectrally well separated from GFP-based probes (excitation and emission peaks at 550 nm and 580 nm, respectively) and is as bright as enhanced GFP (EGFP) at neutral pH. Finally, its excitation spectrum is highly pH sensitive in the appropriate pH range (pK_a 7.8). Accordingly, pHTomato is dim in quiescent vesicles (pH 5.5) but much brighter when the vesicle interior equilibrates with the extracellular medium (pH 7.4).

mOrange2 recently has been applied to image vesicular turnover concurrently with calcium²⁰ or pHluorin probes³⁰, although its pK_a (6.5) could be further optimized to improve signal-to-noise ratio. Other pH-sensitive probes such as mNectarine³¹ and pHRed³² were recently identified, albeit without the explicit motivation of tracking synaptic transmission. mNectarine is less bright than pHTomato, and pHRed undergoes a pH-dependent change spectral shape that could be disadvantageous for concomitant use with other probes though useful for ratiometric imaging. In contrast, sypHTomato, derived from pHTomato, operates on the same principle as synaptopHluorin⁶, and displays comparable performance in culture (**Fig. 1**). If anything, sypHTomato would be better suited than green probes for imaging in brain tissue, where light scattering falls off at longer wavelengths.

Having a red pH-sensitive probe enabled us to perform dual color imaging with another functional indicator to study neural communications in a multiplex fashion. We have demonstrated this potential use in two ways. First, we were able to image sypHTomato together with GCaMP3 in the same cellular region. We were able to visualize activity-dependent calcium signals and the corresponding vesicular turnover with single-synapse resolution. This spatial resolution allowed us to study how different populations of voltage-gated Ca^{2+} channels scale according to the presynaptic size. We found that the deployment of P/Q- and N-type channels was notably consistent at glutamatergic synapses, despite large size variations between individual presynaptic terminals.

Second, we were able to mark the presynaptic neuron with sypHTomato and read out postsynaptic calcium response reported by GCaMP3. This configuration enabled genetically encoded, the first, to our knowledge, all-optical visualization of chemical presynaptic to postsynaptic transmission at single synapses. We observed a close size matching between pre- and postsynaptic boutons at the single-synapse level, consistent with electron microscopy reconstruction studies from slice tissues²⁷. Of note, we also found that presynaptic terminals tended to have similar presynaptic masses (for example, readily releasable pool or total vesicle pool) if they happened to share the same postsynaptic target. It has been suggested that extrinsic factors such as retrograde signals from postsynaptic neurons³³, local dendritic excitability²⁸ or signals from glial cells³⁴ might regulate the presynaptic release probability. Our results point to new possibilities: presynaptic readily releasable pools or total vesicular pools might also be concurrently regulated. Finally, our ability to visualize pre- and postsynaptic responses under subthreshold or suprathreshold conditions opens doors to perform studies to decipher the locus of pre- or postsynaptic regulation of synaptic strength in slice or *in vivo*.

Perhaps the widest application of dual-color synaptic photometry will involve probing multiple pathways in neural circuits. Here, we have taken a critical first step: combining optogenetic photostimulation with optical monitoring. Our strategy satisfies two important requirements: (i) using a specific light stimulus to drive neuronal firing with channelrhodopsin and to query an optical reporter of neurotransmission and (ii) using a second, distinct optical stimulus to achieve firing and readout of a second pathway without cross-talk with the first. In practical terms, we achieved this by using blue light to trigger spiking with ChR2 and to monitor synaptic activity with GFP-based reporters, and green light to drive VChR1- and pHTomato-based probes in parallel fashion. In principle, this approach can be extended to photo-excitation and monitoring of different classes of neuron *in situ*. Our sypHTomato-based multiplex system could readily be extended to two-photon imaging for in-slice or *in vivo* studies³⁵. Because two-photon excitation is generally ineffective in activating channelrhodopsins³⁶, photostimulation and optical readout could conceivably be controlled independently; for example, using ChR2 in conjunction with sypHTomato (**Supplementary Fig. 6b**). The availability of a red, pH-sensitive synaptic probe provides a key component of more flexible and robust optical platforms for dissecting neural circuits *in situ*.

METHODS

Methods and any associated references are available in the online version of the paper.

Accession codes. GenBank: pHTomato, JQ966306.

Note: Supplementary information is available in the online version of the paper.

ACKNOWLEDGMENTS

We thank M. Lin for help with quantum yield measurements. We thank J. Emery for technical assistance and L. Li for help with transfections. We thank L. Luo and Tsien laboratory members, especially M. Tadross, S. Owen, H. Park and R. Groth, for discussions throughout the execution of this project. This work was supported by grants from the US National Institute of Neurological Disorders and Stroke (NS074785 and NS24067), the US National Institute of Mental Health (MH064070), the Mathers Foundation and the Burnett family fund (to R.W.T.).

AUTHOR CONTRIBUTIONS

Y.L. conceived and performed the experiments. R.W.T. supervised the project. Y.L. and R.W.T. wrote the manuscript.

COMPETING FINANCIAL INTERESTS

The authors declare no competing financial interests.

Published online at <http://www.nature.com/doi/10.1038/nn.3126>.

Reprints and permissions information is available online at <http://www.nature.com/reprints/index.html>.

- Siegel, M.S. & Isacoff, E.Y. A genetically encoded optical probe of membrane voltage. *Neuron* **19**, 735–741 (1997).
- Mutoh, H., Perron, A., Akemann, W., Iwamoto, Y. & Knopfel, T. Optogenetic monitoring of membrane potentials. *Exp. Physiol.* **96**, 13–18 (2011).
- Miyawaki, A. Development of probes for cellular functions using fluorescent proteins and fluorescence resonance energy transfer. *Annu. Rev. Biochem.* **2011**, 357–373 (2011).
- Miyawaki, A. *et al.* Fluorescent indicators for Ca²⁺ based on green fluorescent proteins and calmodulin. *Nature* **388**, 882–887 (1997).
- Kuner, T. & Augustine, G.J. A genetically encoded ratiometric indicator for chloride: capturing chloride transients in cultured hippocampal neurons. *Neuron* **27**, 447–459 (2000).
- Miesenböck, G., De Angelis, D.A. & Rothman, J.E. Visualizing secretion and synaptic transmission with pH-sensitive green fluorescent proteins. *Nature* **394**, 192–195 (1998).
- Miesenböck, G. & Kevrekidis, I.G. Optical imaging and control of genetically designated neurons in functioning circuits. *Annu. Rev. Neurosci.* **28**, 533–563 (2005).
- Chow, B.Y. *et al.* High-performance genetically targetable optical neural silencing by light-driven proton pumps. *Nature* **463**, 98–102 (2010).
- Zhang, F. *et al.* Red-shifted optogenetic excitation: a tool for fast neural control derived from *Volvox carterii*. *Nat. Neurosci.* **11**, 631–633 (2008).
- Boyden, E.S., Zhang, F., Bamberg, E., Nagel, G. & Deisseroth, K. Millisecond-timescale, genetically targeted optical control of neural activity. *Nat. Neurosci.* **8**, 1263–1268 (2005).
- Shaner, N.C. *et al.* Improving the photostability of bright monomeric orange and red fluorescent proteins. *Nat. Methods* **5**, 545–551 (2008).
- Kremers, G.J., Hazelwood, K.L., Murphy, C.S., Davidson, M.W. & Piston, D.W. Photoconversion in orange and red fluorescent proteins. *Nat. Methods* **6**, 355–358 (2009).
- Shcherbo, D. *et al.* Bright far-red fluorescent protein for whole-body imaging. *Nat. Methods* **4**, 741–746 (2007).
- Sankaranarayanan, S., De Angelis, D., Rothman, J.E. & Ryan, T.A. The use of pHluorins for optical measurements of presynaptic activity. *Biophys. J.* **79**, 2199–2208 (2000).
- Campbell, R.E. *et al.* A monomeric red fluorescent protein. *Proc. Natl. Acad. Sci. USA* **99**, 7877–7882 (2002).
- Shaner, N.C. *et al.* Improved monomeric red, orange and yellow fluorescent proteins derived from *Discosoma* sp. red fluorescent protein. *Nat. Biotechnol.* **22**, 1567–1572 (2004).
- Jach, G., Pesch, M., Richter, K., Frings, S. & Uhrig, J.F. An improved mRFP1 adds red to bimolecular fluorescence complementation. *Nat. Methods* **3**, 597–600 (2006).
- Granseth, B., Odermatt, B., Royle, S.J. & Lagnado, L. Clathrin-mediated endocytosis is the dominant mechanism of vesicle retrieval at hippocampal synapses. *Neuron* **51**, 773–786 (2006).
- Zhu, Y., Xu, J. & Heinemann, S.F. Two pathways of synaptic vesicle retrieval revealed by single-vesicle imaging. *Neuron* **61**, 397–411 (2009).
- Li, H. *et al.* Concurrent imaging of synaptic vesicle recycling and calcium dynamics. *Front. Mol. Neurosci.* **4**, 34 (2011).
- Tian, L. *et al.* Imaging neural activity in worms, flies and mice with improved GCaMP calcium indicators. *Nat. Methods* **6**, 875–881 (2009).
- Boron, W.F. & De Weer, P. Intracellular pH transients in squid giant axons caused by CO₂, NH₃, and metabolic inhibitors. *J. Gen. Physiol.* **67**, 91–112 (1976).
- Reuter, H. Measurements of exocytosis from single presynaptic nerve terminals reveal heterogeneous inhibition by Ca²⁺-channel blockers. *Neuron* **14**, 773–779 (1995).
- Reid, C.A., Clements, J.D. & Bekkers, J.M. Nonuniform distribution of Ca²⁺ channel subtypes on presynaptic terminals of excitatory synapses in hippocampal cultures. *J. Neurosci.* **17**, 2738–2745 (1997).
- Murthy, V.N. & Stevens, C.F. Reversal of synaptic vesicle docking at central synapses. *Nat. Neurosci.* **2**, 503–507 (1999).
- Pierce, J.P. & Lewin, G.R. An ultrastructural size principle. *Neuroscience* **58**, 441–446 (1994).
- Harris, K.M. & Stevens, J.K. Dendritic spines of CA 1 pyramidal cells in the rat hippocampus: serial electron microscopy with reference to their biophysical characteristics. *J. Neurosci.* **9**, 2982–2997 (1989).
- Branco, T., Staras, K., Darcy, K.J. & Goda, Y. Local dendritic activity sets release probability at hippocampal synapses. *Neuron* **59**, 475–485 (2008).
- Voglmaier, S.M. *et al.* Distinct endocytic pathways control the rate and extent of synaptic vesicle protein recycling. *Neuron* **51**, 71–84 (2006).
- Ramirez, D.M., Khvotchev, M., Trauterman, B. & Kavalali, E.T. Vti1a identifies a vesicle pool that preferentially recycles at rest and maintains spontaneous neurotransmission. *Neuron* **73**, 121–134 (2012).
- Johnson, D.E. *et al.* Red fluorescent protein pH biosensor to detect concentrative nucleoside transport. *J. Biol. Chem.* **284**, 20499–20511 (2009).
- Tantama, M., Hung, Y.P. & Yellen, G. Imaging intracellular pH in live cells with a genetically encoded red fluorescent protein sensor. *J. Am. Chem. Soc.* **133**, 10034–10037 (2011).
- Micheva, K.D., Buchanan, J., Holz, R.W. & Smith, S.J. Retrograde regulation of synaptic vesicle endocytosis and recycling. *Nat. Neurosci.* **6**, 925–932 (2003).
- Auld, D.S. & Robitaille, R. Glial cells and neurotransmission: an inclusive view of synaptic function. *Neuron* **40**, 389–400 (2003).
- Helmchen, F. & Denk, W. Deep tissue two-photon microscopy. *Nat. Methods* **2**, 932–940 (2005).
- Rickgauer, J.P. & Tank, D.W. Two-photon excitation of channelrhodopsin-2 at saturation. *Proc. Natl. Acad. Sci. USA* **106**, 15025–15030 (2009).
- Shaner, N.C., Steinbach, P.A. & Tsien, R.Y. A guide to choosing fluorescent proteins. *Nat. Methods* **2**, 905–909 (2005).

ONLINE METHODS

Molecular biology and protein purification. mRFP/mStrawberry and GCaMP3 constructs were kindly provided by R.Y. Tsien (University of California, San Diego) and L. Looger (Janelia Farms), respectively. ChR2/vChR1, sypH and vGluT_{PH} were kindly provided by K. Deisseroth (Stanford), Y. Zhu (Northwestern University) and R.H. Edwards (University of California, San Francisco), respectively.

Evolution of pHTomato was carried out by error-prone PCR (epPCR) using GeneMorph II kit with equal amounts of mRFP and mStrawberry as templates. After DpnI treatment, the amplified fragment was cloned into pBAD/His vector (Invitrogen, Carlsbad) and transformed into 10G Supreme electrocompetent cells (Lucigen, WI). Two additional rounds of epPCR were performed using a pool template that came from a collection of previous transformed colonies (~300 colonies each time). Before final selection, single bacterial colonies were cultured overnight in 96-well plates induced with 0.2% arabinose (w/v, in LB). Screening for pH sensitivity was performed with a fluorescence plate reader (FLEXstation II, Molecular Devices, CA) with excitation and emission wavelengths set at 540 and 590 nm, respectively. Emission ratios were calculated from data obtained from 576 individual colonies in the presence of PBS (pH 7.4) or PBS plus 60 mM sodium acetate (pH 5.0, $pK_a = 4.7$). Plasmids from bacteria with higher ratios were extracted and sequenced.

VAMP2-pHTomato was created by PCR insertion of pHTomato into the C terminal of VAMP2 so that it would face the lumens of synaptic vesicles. SypHTomato was created by insertion of pHTomato between positions 184 and 185 of rat synaptophysin sequence as previously described¹⁹. Mammalian expression vectors for sypHTomato, vGluT_{PH}, ChR2 and VChR1 were first subcloned into pDONR221 or pDONR-P2R-P3 plasmids to generate entry vectors and later assembled with a CMV promoter (in HEK cells or neurons) or α CaMKII promoter (in neurons) by the LR recombination reaction (Multisite Gateway, Invitrogen). T2A linkers were inserted into entry vectors of vGluT_{PH} or sypHTomato by mutagenesis (Change-IT, USB).

Recombinant His-tagged pHTomato or EGFP were purified by Ni-NTA chromatography (Qiagen). Spectral measurements of pHTomato were performed with a FluoroMax3 spectrofluorometer (Horiba, NJ) with peak of excitation set at 550 nm and emission set at 580 nm. Titration of pH was performed with a series of precalibrated PBS or PBS + 60 mM sodium acetate solutions. Quantum yield measurements were done in a Safire² system (Tecan) using rhodamine 6G (QY = 0.95 in ethanol) as a reference.

Cell culture and transfections. CA3-CA1 hippocampal neurons were cultured as previously described³⁸. Both HEK cells and neurons were transfected with DNA by calcium phosphate methods. For cotransfections, same amount of sypH and sypHTomato driven by CMV promoter were used. For sequential transfections, individual plasmids were separated mixed with calcium chloride and phosphate buffer and applied to neuron sequentially with interval of 2–24 h. Neurons were typically transfected after 7–9 d *in vitro* and experiments performed at 14–21 d *in vitro*.

Imaging, electrical and optical stimulation. Neurons were perfused with Tyrode solution (containing 150 mM NaCl, 4 mM KCl, 2 mM CaCl₂, 2 mM MgCl₂, 10 mM glucose, 10 mM HEPES, 310–315 mOsm, with pH at 7.35). Switching of perfusion solution was carried out with a precision of <2 s. In some experiments, solutions contained 10 μ M NBQX and 50 μ M D-APV (Tocris Bioscience) to prevent possible recurrent activity and synaptic plasticity. HEK cells were perfused with Tyrode with non-membrane-permeable MES buffer (50 mM, $pK_a = 6.1$) or PBS to gauge the pH dependence of surface VAMP2-pHTomato intensity. Surface fraction of VAMP2-pHTomato is about 25% of the total protein measured by detergent permeabilization experiments (0.1% Triton X-100). For the pair imaging, control solution was similar to the Tyrode except with 0 mM MgCl₂ and 5 μ M glycine to prevent the block of NMDA receptors. A sypHTomato-positive neuron was stimulated by a glass pipette or a concentric bipolar electrode (FHC) placed close to the soma of the neuron with a current strength of ~1 mA. For field stimulation, neurons were stimulated by 40 mA current passing through platinum electrodes. 1 ms pulse with different duration was applied. All experiments were performed at room temperature.

Image acquisition was conducted as previously described³⁸. Briefly, neurons were imaged on a Nikon TE2000 microscope (40 \times , 1.3 NA objective) with an EMCCD camera (Cascade512B, Roper Scientific), controlled by METAMORPH

7.0 Software (Universal Imaging). Dual color imaging of sypHTomato and GCaMP3 was accomplished by using two excitation filters (475/22 for GCaMP3 and 556/20 for pHTomato). For light stimulation/imaging experiments, blue light excitation filter (FF438/24, Semrock) at an intensity 0.7–3 mW mm⁻² (measured by a digital light meter, CETO) and orange light excitation filter at 1–4 mW mm⁻² (556/20, Chroma) were used to excite ChR2/vGluT_{PH} and vChR1/sypHTomato respectively. A dual-band dichroic mirror (FF493/574-Di01, Semrock) and a dual band emitter centered at 512 nm and 630 nm, respectively (FF01-512/630-25, Semrock), were used to collect fluorescence light. The attenuation of excitation light intensity and/or switching between exciters was controlled by a DG4 (Sutter Instruments). The switching time between two channels was <2 ms. Exposure times were typically 40–250 ms, and images were collected at 1–10 Hz. Cross-talk between pHTomato and GCaMP3 channels was measured to be less than 6%. Photobleaching of pHluorin, GCaMP3 or pHTomato was corrected for by linear fitting of the baseline, as validated by experiments in the presence of 100 μ M CdCl₂.

Imaging analysis. Images were analyzed by using ImageJ (NIH) and METAMORPH 7.0 Software (Universal Imaging). Regions of interests were identified by NH₄Cl application (50 mM, pH 7.4), 600 stimuli at 10 Hz or ionomycin application. NH₄Cl is in equilibrium with H⁺ and NH₃. Uncharged NH₃ rapidly diffuses through the plasma membrane and neutralizes the acidic pH in synaptic vesicles. The mask used is a circular selection of 9 pixels (~2 μ m). ROIs with fluorescence increases >3 s.d. larger than neighboring background regions were selected and applied to all the rest of protocols. ROI data were extracted as ASCII files and further processed by Origin 7.0 (OriginLab, MA) or Matlab (MathWorks, MA). To effectively remove the background autofluorescence, in some experiments the images for sypHTomato and GCaMP3 channels were processed by calculating the intensity difference before and after NH₄Cl or ionomycin application respectively.

Calcium calibration. To calibrate the cytosolic calcium signal, F_{\min} and F_{\max} of GCaMP3 were obtained inside the same boutons at the end of the experiments using methods similar to those described before^{39,40}. F_{\min} was obtained by treating the cells with 5 mM EGTA along with 10 μ M ionomycin, and F_{\max} was obtained by treating the cells with the mixtures of 1 mM Ca²⁺ and 10 μ M ionomycin. The *in situ* F_{\min} and F_{\max} values were used to convert live cell data to the absolute calcium concentration using the formula

$$([Ca^{2+}]/K_d)^n = (f/F_{\max} - 1/R_f)/(1 - f/F_{\max}) \quad (1)$$

where $R_f = F_{\max}/F_{\min}$, K_d , R_f and n are inherent properties of the sensors. The K_d (133 \pm 30 nM), R_f (6.1 \pm 2.1) and n (3.9 \pm 0.6) were obtained by least-squares fitting of data from 11 cells to equation (1). The K_d and Hill coefficient were consistent with values previously reported for GCaMP2 and GCaMP3 (ref. 21).

We performed *in situ* calibrations to test whether 40 stimuli at 20 Hz would saturate bulk calcium concentration reported by GCaMP3. Both stimulation for longer durations (60 stimuli at 20 Hz, Fig. 2c) or at higher frequency (40 stimuli at 50 Hz) elicited larger responses, indicating that GCaMP3 signal reflecting the volume average [Ca²⁺] had not reached a ceiling. In addition, retrospective calibration in ionomycin (1 μ M free Ca²⁺) yielded a larger fluorescence response, larger than that reflecting the peak [Ca²⁺]_{pre} (380 nM), again consistent with non-saturated [Ca²⁺]_{pre}. Conservative calculation of the bulk Ca²⁺ level based on the calibration curve and the s.d. of the GCaMP3 signal⁴⁰ indicate the maximal underestimation of calcium level would be no larger than 30%.

Statistics. Coefficient of variation = s.d./mean. Shapiro-Wilk test was performed in Matlab (MathWorks, MA).

38. Zhang, Q., Li, Y. & Tsien, R.W. The dynamic control of kiss-and-run and vesicular reuse probed with single nanoparticles. *Science* **323**, 1448–1453 (2009).
39. Kao, J.P., Harootyan, A.T. & Tsien, R.Y. Photochemically generated cytosolic calcium pulses and their detection by fluo-3. *J. Biol. Chem.* **264**, 8179–8184 (1989).
40. Maravall, M., Mainen, Z.F., Sabatini, B.L. & Svoboda, K. Estimating intracellular calcium concentrations and buffering without wavelength ratioing. *Biophys. J.* **78**, 2655–2667 (2000).